Chapter

Electron and Phonon Transport Mechanisms in Thermoelectric Materials

Hong Liu and Xinli Cheng

Abstract

Thermoelectric materials can directly convert thermal energy into electrical energy. Although the low efficiency of thermoelectric devices limits their use in the professional market, the development and improvement of condensed matter physics theory, as well as the emergence of various new material synthesis processes, have brought new research and development momentum to the utilization of thermoelectric materials. This chapter first starts from the basic theory of thermoelectricity, introduces the thermoelectric transport equation and the Boltzmann transport equation that controls phonon and electron transport, and then reviews the strategies to further improve the thermoelectric properties of materials in the past two decades. and evaluated the effectiveness and universality of existing strategies, pointing out their limitations. Subsequently, based on the superconducting Bardeen-Cooper-Schrieffer (BCS) theory and phonon drag effect, this chapter proposes a new physical paradigm different from the phonon-glass-electron-crystal method. The core of the new paradigm is to shift from decoupling the electron-phonon transport process to optimizing the electron-phonon coupling mechanism and provides a theoretical mechanism for improving the performance of thermoelectric materials by optimizing the electron-phonon coupling. Identified the material design concepts and challenges for implementing the new paradigm.

Keywords: thermoelectricity, Boltzmann transport equation, physical paradigm, electron-phonon coupling, phonon drag effect

1. Introduction

Thermoelectric technology, characterized by direct thermoelectric conversion, is increasingly recognized as a key component of emerging green energy technologies. In order to make thermoelectric equipment more economical and efficient, we must improve the energy conversion efficiency, which is evaluated by the material quality factor (ZT). $ZT = S^2 \sigma T/\kappa$ [1] depends on conductivity (σ), Seebeck coefficient (S), and thermal conductivity (κ, sum of phonon κ_l and electron κ_e components). ZT enhancement is typically achieved by increasing the power factor ($S^2 \sigma$) and decreasing κ_l, which correspond to charge carrier transport and phonon propagation,

respectively, and which is challenging as these requirements are often contradictory to each other in conventional materials [2].

High-performance thermoelectric materials rely on innovative thermoelectric transport mechanisms. Related strategies include the quantum confinement effect [3], resonant energy levels [4], band convergence [5], liquid ions [6], entropy engineering [7], anharmonicity [8], modulation doping [9], spin orbit coupling (SOC) [10], and Rashba effect [11], which enhance ZT in many thermoelectric material systems. However, the research progress on enhancing thermoelectric material ZT seems to have only partial and minor success. In order to further promote the development of thermoelectric materials, exploring the paradigm shift mechanism is crucial. This chapter will start from the basic theory of thermoelectricity and explore new thermoelectric transport mechanisms, highlighting the main physical parameters and related description methods that affect electron and phonon transport processes, providing new prospects for manipulating thermoelectric properties. Firstly, briefly introduce the basic principles of thermoelectric devices and materials (Section 2), and then summarize the current status of the optimization mechanism of thermoelectric transport in thermoelectric materials (Section 3). Then, we will discuss the thermoelectric transport mechanism in bulk materials, as well as the physical paradigm for synergistically reducing the thermal conductivity and improving the power factor of bulk materials (Section 4), and finally present the conclusions of this chapter (Section 5).

2. Thermoelectric transport

2.1 Transport equation in thermoelectric materials

The electrical and thermal transport processes in thermoelectric materials are not independent but interact with each other. Essentially, the charges in semiconductors and conductors carry away heat during their movement. The interrelated current density J_e and heat flux density J_q can be expressed as [12, 13]

$$J_e = L_{11}\left(-\frac{d\Phi}{dx}\right) + L_{12}\left(-\frac{dT}{dx}\right) \tag{1}$$

$$J_q = L_{21}\left(-\frac{d\Phi}{dx}\right) + L_{22}\left(-\frac{dT}{dx}\right) \tag{2}$$

Consider one-dimensional transport, where L_{11} is the conductivity and Φ is the potential, which is the electrochemical potential per unit charge. In an isothermal conductor, heat flux can be expressed as

$$J_q = \frac{L_{21}}{L_{11}} J_e = \Pi J_e \tag{3}$$

Proportional to the current, the proportionality constant is the Peltier coefficient Π. Although the Peltier coefficient is an inherent material property, as shown in **Figure 1**, due to the imbalance of Peltier heat between the inflow and outflow junctions, Peltier cooling and heating occur when two materials with different Peltier coefficients are connected together. Control volume analysis shows that the cooling or heating Q occurring at the junction is equal to

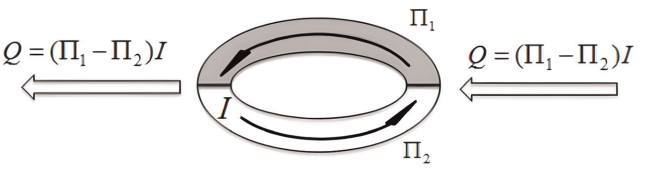

Figure 1.
Cooling or heating at the junctions of two materials occur because of the different Peltier coefficients of the two materials, which can be used as thermoelectric refrigerators or heat pumps.

$$Q = (\Pi_2 - \Pi_1)I \tag{4}$$

In Eq. (4), I is the current, and Π_1 and Π_2 represent the Peltier coefficients of the two materials. According to the definition of the Seebeck coefficient, taking $J_e = 0$ in Eq. (1), the Seebeck coefficient can be obtained as

$$S = \frac{-d\Phi/dx}{dT/dx} = -\frac{V}{\Delta T} = \frac{L_{12}}{L_{11}} \tag{5}$$

As shown in Eq. (5), the Seebeck voltage V between two points on a uniform material is independent of temperature distribution. Thermocouples measure temperature based on this material characteristic.

The Seebeck coefficient and the Peltier coefficient are not independent but interrelated and are expressed as $\Pi = TS$, this is also a generalized Onsager reciprocity relationship $L_{21} = TL_{12}$.

Furthermore, one can eliminate the electrochemical potential in Eq. (1) and express the heat current as

$$J_q = \Pi J_e - \kappa_e \frac{dT}{dx} \tag{6}$$

where the electronic contribution to thermal conductivity is

$$\kappa_e = L_{22} - \frac{L_{12}L_{21}}{L_{11}} \tag{7}$$

The transport coefficient can be further correlated with the electronic band structure of the material. Based on the Linearized Boltzmann Transport Equation (LBTE) formalism under the relaxation time approximation, the transport coefficient of isotropic materials with a single energy band can be expressed as [14].

$$L_{11} = -\frac{e^2}{3}\int v^2 \tau \frac{\partial f^0}{\partial E} N(E) dE \tag{8}$$

$$L_{12} = \frac{e^2}{3T}\int v^2 \tau (E - E_f) \frac{\partial f^0}{\partial E} N(E) dE \tag{9}$$

$$L_{22} = -\frac{1}{3T}\int v^2 \tau (E - E_f)^2 \frac{\partial f^0}{\partial E} N(E) dE \tag{10}$$

Among them, τ is the relaxation time, $N(E)$ is the density of electronic states per unit volume per unit energy interval, f^0 is the Fermi Dirac distribution in equilibrium

state, and E_f is the electrochemical potential based on doping modulation. According to Eqs. (5), (8), and (9), the Seebeck coefficient can be expressed as

$$S = -\frac{1}{eT}\frac{\int v^2\tau\left(E - E_f\right)\frac{\partial f^0}{\partial E}N(E)dE}{\int v^2\tau\frac{\partial f^0}{\partial E}N(E)dE} \tag{11}$$

According to Eqs. (1) and (2), considering a virtual process that does not generate temperature gradients, we can obtain: $\frac{J_q/T}{J_e} = S$, this means that the Seebeck coefficient is the entropy current carried by a unit current density. Moreover, temperature gradient (phonon non-equilibrium distribution) can generate non-uniform distribution of charge carriers and form potential gradient, and similarly, potential gradient (charge carrier non-equilibrium distribution) can lead to non-uniform distribution of phonons and form temperature gradient. Explanation of the evolutionary mechanisms for phonon non-equilibrium distribution and charge carrier non-equilibrium distribution in sections 2.2 and 2.3.

2.2 Boltzmann transport equation for phonon

The non-zero heat flux J can be generated by a temperature gradient of ∇T. Within the linear range, the component of thermal conductivity κ is determined by the following equation $J^\alpha = -\sum_\beta \kappa^{\alpha\beta}(\nabla \mathrm{T})^\beta$. $\boldsymbol{J}$ can be obtained through the following methods

$$\boldsymbol{J} = \sum_p \int f_\lambda \hbar\omega_\lambda \boldsymbol{v}_\lambda \frac{d\boldsymbol{q}}{(2\pi)^3} \tag{12}$$

Among them, λ is the phonon mode identifier, including phonon branching index p and wave vector q, ω_λ and $\boldsymbol{v}_\lambda$ are the angular frequency and group velocity of phonon mode λ, respectively, and f_λ is the corresponding phonon distribution function. In the state of thermal equilibrium without thermodynamic forces, the distribution of phonons is determined by the Bose-Einstein statistical distribution function $f_0(\omega_\lambda)$. When a temperature gradient of ∇T occurs, the distribution function f deviates from f_0, and the deviation can be obtained by iteratively solving the Boltzmann transport equation. The variation of the phonon distribution function comes from diffusion caused by ∇T and scattering caused by related mechanisms. When reaching steady state, the time rate of change of the distribution function is 0; The corresponding relationship can be expressed as [15]:

$$\frac{df_\lambda}{dt} = \frac{\partial f_\lambda}{\partial f}|_{diffusion} + \frac{\partial f_\lambda}{\partial f}|_{scattering} \tag{13}$$

where,

$$\frac{\partial f_\lambda}{\partial f}|_{diffusion} = -\nabla T \bullet \boldsymbol{v}_\lambda \frac{\partial f_\lambda}{\partial T} \tag{14}$$

and $\frac{\partial f_\lambda}{\partial f}|_{scattering}$ depending on the relevant scattering process, analyze and solve using perturbation theory. The phonon scattering in single crystal materials mainly comes from phonon-phonon scattering and impurity scattering such as isotopes. In addition,

the size of actual block samples is always limited to the extent that boundary scattering dominates at very low temperatures.

In most cases, the norm of ∇T is small enough that f_λ can be expanded to the first-order term of ∇T, that is $f_\lambda = f_0(\omega_\lambda) + g_\lambda$, where g_λ depends on ∇T linearly. We can choose to express this dependence as $g_\lambda = -F_\lambda \nabla T \, df_0/dT$. When the scattering process is two phonons and three phonons, the linearized Boltzmann equation is [16]:

$$F_\lambda = \tau_\lambda^0 \left(\boldsymbol{v}_\lambda + \Delta_\lambda\right) \tag{15}$$

In Eq. (15), τ_λ^0 is the relaxation time of the mode λ obtained from perturbation theory, which is commonly used in relaxation time approximation (RTA). Setting all Δ_λ to zero in Eq. (15) is equivalent to working in RTA. Therefore, the dimension of Δ_λ with velocity is a measure of the degree to which a population of specific phonon modes (and associated heat flux) deviates from RTA predictions. The calculation formula for Δ_λ and τ_λ^0 is

$$\Delta_\lambda = \frac{1}{N}\sum_{\lambda'\lambda''}^{+} \Gamma^+_{\lambda\lambda'\lambda''}\left(\xi_{\lambda\lambda''}\mathbf{F}_{\lambda''} - \xi_{\lambda\lambda'}\mathbf{F}_{\lambda'}\right) + \frac{1}{N}\sum_{\lambda'\lambda''}^{-} \frac{1}{2}\Gamma^-_{\lambda\lambda'\lambda''}\left(\xi_{\lambda\lambda''}\mathbf{F}_{\lambda''} - \xi_{\lambda\lambda'}\mathbf{F}_{\lambda'}\right) + \frac{1}{N}\sum_{\lambda'} \Gamma_{\lambda\lambda'}\xi_{\lambda\lambda'}\mathbf{F}_{\lambda'} \tag{16}$$

$$\frac{1}{\tau_\lambda^0} = \frac{1}{N}\left(\sum_{\lambda'\lambda''}^{+} \Gamma^+_{\lambda\lambda'\lambda''} + \sum_{\lambda'\lambda''}^{-} \frac{1}{2}\Gamma^-_{\lambda\lambda'\lambda''} + \sum_{\lambda'} \Gamma_{\lambda\lambda'}\right) \tag{17}$$

We discretize the Brillouin zone (BZ) into a regular grid of N=N1 × N2 × N3 q-points centered on Γ and use the abbreviation $\xi_{\lambda\lambda'} = \omega_{\lambda'}/\omega_\lambda$. In $\sum^{\pm}$ summation, the conservation of quasi-momentum requires $\mathbf{q}'' = \mathbf{q} \pm \mathbf{q}' + \mathbf{Q}$, which maps $\mathbf{q}''$ to the first Brillouin zone through translational reciprocal-lattice vector $\mathbf{Q}$. The symbols used here are slightly different from those used by some authors [17] in previous publications, where group velocity was not included in Δ_λ.

The quantity $\Gamma^{\pm}_{\lambda\lambda'\lambda''}$ in Eq. (17) is the scattering rate in the three-phonon process, which can be expressed as

$$\Gamma^+_{\lambda\lambda'\lambda''} = \frac{\hbar\pi}{4}\frac{f_0' - f_0''}{\omega_\lambda\omega_{\lambda'}\omega_{\lambda''}}\left|V^+_{\lambda\lambda'\lambda''}\right|^2\delta(\omega_\lambda + \omega_{\lambda'} - \omega_{\lambda''}) \tag{18}$$

$$\Gamma^-_{\lambda\lambda'\lambda''} = \frac{\hbar\pi}{4}\frac{f_0' + f_0'' + 1}{\omega_\lambda\omega_{\lambda'}\omega_{\lambda''}}\left|V^-_{\lambda\lambda'\lambda''}\right|^2\delta(\omega_\lambda - \omega_{\lambda'} - \omega_{\lambda''}) \tag{19}$$

To simplify the representation, f_0' refers to table $f_0(\omega_{\lambda'})$, and so on. $\Gamma^+_{\lambda\lambda'\lambda''}$ corresponds to the absorption process, where two phonons combine into one phonon, corresponding to energy $(\omega_\lambda + \omega_{\lambda'} = \omega_{\lambda''})$. The conservation of energy during absorption and emission is limited by the Dirac delta distribution in Eqs. (18) and (19). In order to calculate the value of $\Gamma^{\pm}_{\lambda\lambda'\lambda''}$, it is necessary to provide the scattering matrix element $V^{\pm}_{\lambda\lambda'\lambda''}$, which is given by [16].

$$V^{\pm}_{\lambda\lambda'\lambda''} = \sum_{i\in u.c}\sum_{j,k}\sum_{\alpha\beta\gamma}\Phi^{\alpha\beta\gamma}_{ijk}\frac{e^\alpha_\lambda(i)e^\beta_{p',\pm q'}(j)e^\gamma_{p'',-q''}(k)}{\sqrt{M_iM_jM_k}} \tag{20}$$

these in turn depend on the normalized eigenfunctions $\boldsymbol{e}_{p,q}$ of the three phonons involved and on the anharmonic IFCs $\boldsymbol{\Phi}_{ijk}^{\alpha\beta\gamma} = \frac{\partial^3 E}{\partial r_i^\alpha \partial r_j^\beta \partial_k^\gamma}$. In Eq. (20), i, j, and k represent atomic indices, while α, β, and γ represent Cartesian coordinates. The summation index i only traverses the atoms in the central unit cell, while j and k cover the entire system. r_i^α and M_i represent the alpha component of the displacement from the equilibrium position and the mass of the i-th atom, respectively. $e_\lambda^\alpha(i)$ is the alpha component of the mode λ eigenfunction at the i-th atom.

The above analysis process is based on particle models to calculate the diffusion and scattering mechanisms of phonons, without involving the wave characteristics of interface adaptation. The phonon transport mechanism in nanostructures is of great significance for the precise customization of thermal properties. By combining phonon particles and wave effects through different strategies, the study aims to achieve ultra-low or ultra-high thermal conductivity in various nanostructures. However, phonon particles and wave effects are coupled together, so their respective contributions to phonon transport have not yet been calculated clearly. It is generally believed that the wave effect is the main modulator that blocks phonon transport, and the particle effect is so weak that it can be ignored, but this may not be the case in reality.

In addition, the interaction between electrons and phonons can also affect the transport properties of phonons. The above analytical process only used the potential energy surface of electrons when calculating the interaction force constant using density functional perturbation theory (DFPT). The influence of electron-phonon interaction on phonon transport will be introduced in Section 4.3.2.

2.3 Boltzmann transport equation for electron

Assuming a solid with a temperature gradient, it can be inferred that the chemical potential at the hot end is lower than that at the cold end. Adding an electron requires less energy, and the electron naturally migrates toward the hot end. This provides another explanation for the thermoelectric phenomenon, where a thermal gradient can generate voltage without a net current. Because electrons are governed by two equilibrium forces: one is the so-called "thermal" force that pushes electrons from the cold end to the hot end, and the other is the opposite so-called "electric" force. Therefore, the thermoelectric phenomenon can be considered as a result of the temperature dependence of chemical potential, which is itself a result of the Fermi-Dirac distribution thermal broadening. **Figure 2** depicts the semiclassical picture of the thermoelectric effect.

The Boltzmann equation, a method historically used to calculate the transport coefficients of bulk materials in the Drude model [13, 15, 18].

The core concept in Boltzmann transport theory is the non-equilibrium distribution function $f_k(\boldsymbol{r})$, defined as the number of electrons per unit volume near the $(\boldsymbol{r}, \boldsymbol{k})$ phase space (in fact, the time, energy band, and spin are also specified, which have been omitted for simplicity). In the case of thermal equilibrium, where the temperature is uniform and there is no external field effect, the distribution function and equilibrium distribution function f^0 agrees.

When there is an external field, the distribution function will change due to the acceleration of electrons by the field (the wave vector distribution is no longer symmetrical); In addition, the distribution function may depend on location (non-uniformity in spatial distribution, such as temperature gradients, density gradients,

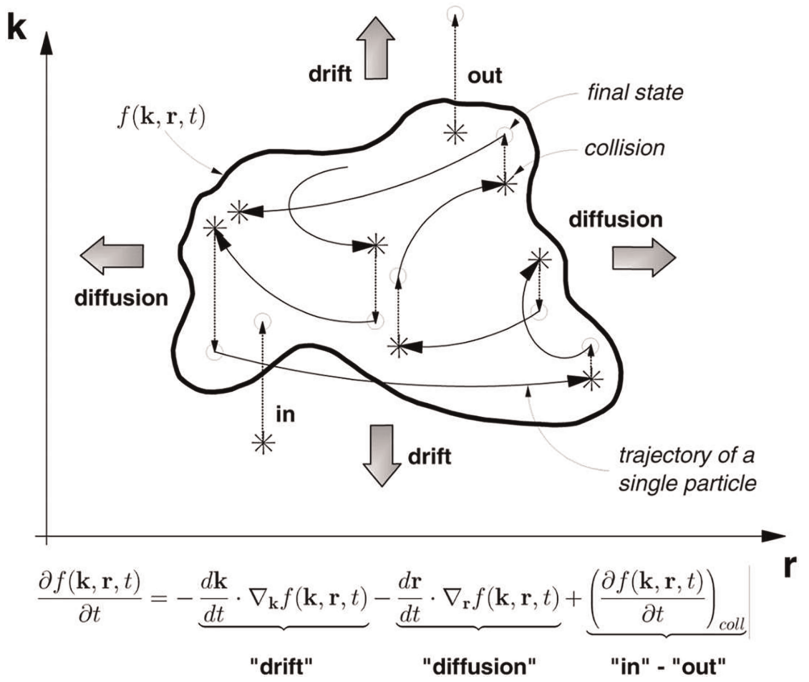

Figure 2.
The semi classical picture of thermoelectric effect.

etc.), which can occur when electrons have a tendency to diffuse; The third effect that causes changes in the distribution function is scattering—electrons interact with phonons, other electrons, impurities, defects, and surfaces. Therefore, the transport process can be attributed to the influence of external fields (electric fields, magnetic fields, etc.), diffusion, and collision scattering on the electron distribution function, leading to deviations from its relative Fermi-Dirac distribution, and the overall results of these three effects should cancel each other out.

Electron group velocity $\boldsymbol{v_k}$ as

$$\boldsymbol{v_k} = \frac{\partial \boldsymbol{\omega_k}}{\partial \boldsymbol{k}} = \frac{\mathbf{1}}{\hbar}\frac{\partial \boldsymbol{\varepsilon_k}}{\partial \boldsymbol{k}} \tag{21}$$

Current can be written as

$$J_e = \int \boldsymbol{v_k e f_k}(r)\boldsymbol{dk} \tag{22}$$

Energy flow can be written as

$$J_U = \int \boldsymbol{v_k \varepsilon f_k}(r)\boldsymbol{dk} \tag{23}$$

The heat flow (the amount of heat carried by electrons) is

$$J_q = J_U - \mu J_N = \int \boldsymbol{v_k}(\boldsymbol{\varepsilon} - \boldsymbol{\mu})\boldsymbol{f_k}(r)\boldsymbol{dk} \tag{24}$$

Consider the near-equilibrium state (local equilibrium assumption and the time scale of interest Δt satisfy $\tau_{local} \ll \Delta t \ll \tau_{system}$). Based on relaxation time approximation:

$$\frac{df_k(\boldsymbol{r})}{dt}|_{scattering} = \frac{f_k(r) - f^0}{\tau} \tag{25}$$

The diffusion term caused by the temperature gradient is

$$\frac{df_k(\boldsymbol{r})}{dt}|_{Temp.grad} = \frac{d\boldsymbol{r}}{dt} \bullet \frac{\partial f_k(\boldsymbol{r})}{\partial \boldsymbol{r}} = \boldsymbol{v}_k \frac{\partial f_k(\boldsymbol{r})}{\partial \boldsymbol{r}} \approx \boldsymbol{v}_k \bullet \frac{\partial f^0}{\partial \boldsymbol{T}} \nabla T \tag{26}$$

The approximation in the above equation assumes that the influence of the temperature gradient on the distribution function is mainly due to the thermal broadening of the Fermi-Dirac distribution. Between two scattering events, electrons drift under the influence of thermal gradients.

Similarly, the influence of the external electric field on the distribution function can be expressed as

$$\frac{df_k(\boldsymbol{r})}{dt}|_{Elec.field} = \frac{d\boldsymbol{k}}{dt} \bullet \frac{\partial f_k(\boldsymbol{r})}{\partial \boldsymbol{k}} = \frac{e}{\hbar}\mathbf{E} \bullet \frac{\partial f_k(\boldsymbol{r})}{\partial k} \approx e\boldsymbol{v}_k \bullet \frac{\partial f^0}{\partial \boldsymbol{\mathcal{E}_k}}\mathbf{E} \tag{27}$$

Therefore, the linear Boltzmann equation can be written as

$$\boldsymbol{v}_k \bullet \frac{\partial f^0}{\partial \boldsymbol{T}} \nabla T + e\boldsymbol{v}_k \bullet \frac{\partial f^0}{\partial \boldsymbol{\mathcal{E}_k}}\mathbf{E} + \frac{f_k(r) - f^0}{\tau} = 0 \tag{28}$$

The deviation of the local distribution function from the steady state comes from two disturbances, which are called drift terms. As shown in **Figure 3**, small changes in

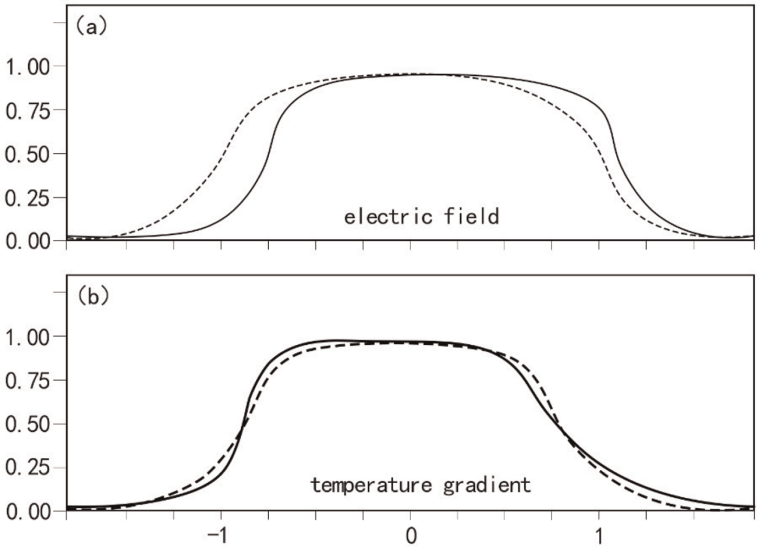

Figure 3.
The distribution function in the presence of an electric field and temperature gradient (the gray line represents the equilibrium distribution).

energy will shift the distribution function, while an increase in temperature will widen the distribution. Therefore, applying an electric field will cause electrons moving in one direction to have greater energy than electrons moving in the opposite direction. On the other hand, in the presence of a thermal gradient, the distribution on the cold side is steeper, and due to the difference in distribution width at both ends of the sample, there is a so-called "heat" that pushes electrons from the cold end to the hot end, which has a significant impact on the physical properties of the system.

According to Eqs. (22) and (28), the conductivity of the system without a thermal gradient is

$$J_e(\nabla T = 0) = \int \left(\boldsymbol{v_k} \boldsymbol{e} f^0 - e^2 \tau \boldsymbol{v}_k^2 \frac{\partial f^0}{\partial \boldsymbol{\mathcal{E}_k}} \mathbf{E} \right) \mathbf{dk} \tag{29}$$

There is no current in thermal equilibrium, so the first term on the right-hand side of the Eq. (29) is integrated to zero, so the conductivity is expressed as

$$\sigma = -\int e^2 \tau(k) \boldsymbol{v}_k^2 \frac{\partial f^0}{\partial \boldsymbol{\mathcal{E}_k}} dk \tag{30}$$

Similarly, in the absence of an electric field, the current density generated by the temperature gradient is

$$J_e(\mathbf{E} = 0) = -\int e\tau \boldsymbol{v}_k^2 \frac{\partial f^0}{\partial T} \nabla T \mathbf{dk} \tag{31}$$

The electrical conductivity generated by heat is derived as follows:

$$\sigma = \int e\tau(k) \boldsymbol{v}_k^2 \frac{\partial f^0}{\partial \boldsymbol{T}} dk \tag{32}$$

Eqs. (30) and (32) clearly demonstrate the k-dependence of relaxation time. How do these two equations tell us the relationship between conductivity generated by electric fields and heat? How are the two related to the Fermi-Dirac distribution? How are the two related to electron velocity and relaxation time? The latter two quantities vary depending on the material and have strong anisotropy.

As can be seen from the above, the conductivity is always positive, while the conductivity generated by heat can be positive or negative. Because $\frac{\partial f^0}{\partial \boldsymbol{\mathcal{E}_k}} = -\frac{1}{k_B T}\left(f^0\right)^2 \exp\left(\frac{\varepsilon-\mu}{k_B T}\right)$ is always negative, $\frac{\partial f^0}{\partial \boldsymbol{T}} = -\frac{\varepsilon-\mu}{T}\frac{\partial f^0}{\partial \boldsymbol{\mathcal{E}_k}}$ depends on $(\varepsilon - \mu)$.

Based on the above discussion, the carriers that play the main role in the two transport processes are different, as shown in **Figure 4**. In the case of charge transport (conductivity), electrons with energy exactly at the chemical potential contribute the most to conductivity (i.e., conductivity mainly depends on the contribution of electrons near the Fermi level); in the case of thermoelectric transport, these carriers do not contribute at all to the thermal conductivity, and the entire signal is determined by electrons with energy slightly higher or lower than the chemical potential, and the contributions of these two parts have opposite signs.

Similar to the above discussion and utilizing the properties of the Fermi-Dirac distribution function, the expression for heat flux can be derived as

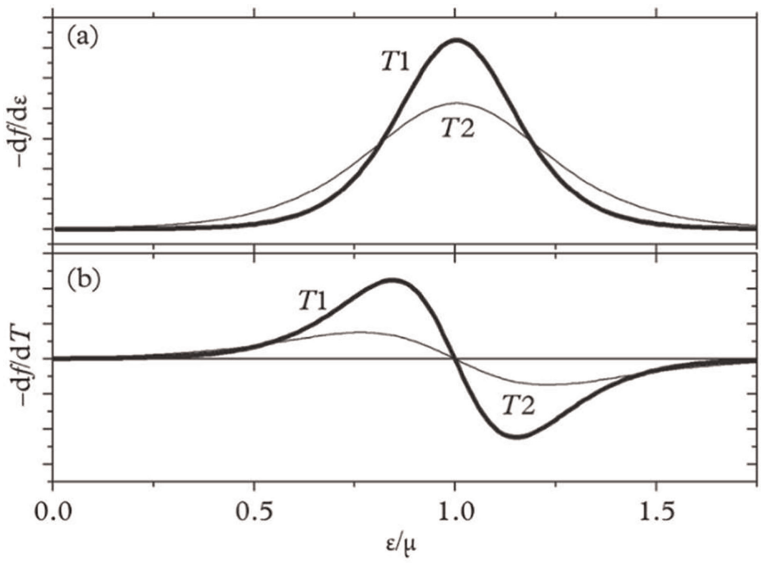

Figure 4.
Two types of derivatives of Fermi distribution, temperature T_1 is less than T_2.

$$J_q = \int \mathbf{v_k}(\boldsymbol{\varepsilon} - \boldsymbol{\mu})\boldsymbol{\tau}\mathbf{v_k}\bullet\left[\frac{(\boldsymbol{\varepsilon} - \boldsymbol{\mu})}{\boldsymbol{T}}\frac{\partial f^0}{\partial \boldsymbol{\mathcal{E}}_k}\nabla T - e\frac{\partial f^0}{\partial \boldsymbol{\mathcal{E}}_k}\mathbf{E}\right]\mathbf{dk} \tag{33}$$

According to the above, the transport coefficients corresponding to Eqs. (8), (9), and (10) can be derived.

The Boltzmann equation is a product of the classical particle Newtonian mechanics model and the quantum mechanics model of energy state transitions. If all coherence effects are ignored and simplified, the Boltzmann equation can be derived from the quantum transport model. The classical transport theory is based on the Boltzmann transport theory, and the basic assumptions of Boltzmann theory include: (i) Electrons and holes are both tiny particles; (ii) The particles are independent of each other, without coherence, and interact with each other through scattering; (iii) Particles can be described using Bloch theory; (iv) Scattering is a transient behavior without temporal and spatial persistence; (v) Only consider the scattering between two particles, without taking into account the combined effects between multiple particles. The Boltzmann transport equation is an equation used in the distribution function method, which is an equation satisfied by the non-equilibrium distribution function $f(k, r, t)$. Solving this equation can obtain $f(k, r, t)$ under different conditions, and then various transport parameters of electrons can be obtained.

The Boltzmann transport equation takes into account the velocity distribution of charge carriers and the directionality of scattering, making it relatively accurate. In the presence of external fields such as electric fields or temperature gradients, the Boltzmann equation can be established based on the drift changes caused by the distribution function due to external fields such as electric fields, magnetic fields, and temperature gradients, as well as the changes caused by scattering. Since the scattering term should be an integral of the scattering probability, the Boltaman equation is a differential integral equation. The solution of this equation is very complex, and

approximation methods are usually used. One commonly used approximation method is the relaxation time approximation.

The Boltzmann equation is a high-dimensional equation with three-dimensional wave vector space (k), three-dimensional real space (r), and one-dimensional time (t), which is difficult to solve and is commonly simulated using Monte Carlo methods.

The difference in the description of heat-carrying phonons and conducting electrons by the Boltzmann transport equation is only reflected in the difference in statistical laws and the dynamic forces of distribution functions deviating from the equilibrium state. Both recover to equilibrium through scattering mechanisms, while phonons and electrons always have mutual influence through the correlation of material structure and environment. Therefore, co-modulating the transport process of both is the fundamental strategy to improve the performance of thermoelectric materials. The fourth section of this chapter will discuss in detail the relevant modulation paradigms.

3. The current status of the optimization mechanism of thermoelectric transport in thermoelectric materials

3.1 Strategy for enhancing Seebeck coefficient

3.1.1 Energy band engineering

Based on the quantum confinement effect of low-dimensional materials on band structure [19, 20], the band structure of materials can be modulated by alloying or chemically doping bulk materials (such as forming resonance energy levels and generating band convergence), thereby improving thermoelectric performance.

3.1.1.1 Resonance energy levels

Mahan and Sofo [21] believe that electronic systems with narrow energy distributions during transport can maximize thermoelectric performance. The so-called resonant energy level is called the "virtual bound state" [22–24], similar to the required delta-shaped energy level proposed by Mahan and Sofo [21]. Unlike doping in the bandgap to form electronic energy levels, resonant dopants will generate electronic energy levels located above the conduction band edge or below the valence band edge as shown in **Figure 5** [25], which will significantly alter the electronic density of states of the host material. The state of a resonant energy level is characterized by the energy of the resonant energy level (E_D) and the width of the resonant state (Γ).

The Bethe-Sommerfeld expansion for the Seebeck coefficient can be expressed as [25].

$$S = \frac{\pi^2}{3}\frac{k_B}{e}(k_B T)\left[\frac{1}{n(E)}\frac{dn(E)}{E} + \frac{1}{\mu(E)}\frac{d\mu(E)}{dE}\right] \tag{34}$$

Clearly, the Seebeck coefficient depends on the density of states and the carrier scattering mechanism. Resonance energy levels can provide additional energy states to the main band and increase the effective band mass (m_b), thereby increasing the density-of-states effective mass (m_d^*) [4], where $m_d^* = N_V^{2/3} m_b$ and N_V is the band degeneracy. Additionally, carrier scattering can generate a carrier filtering effect [26, 27].

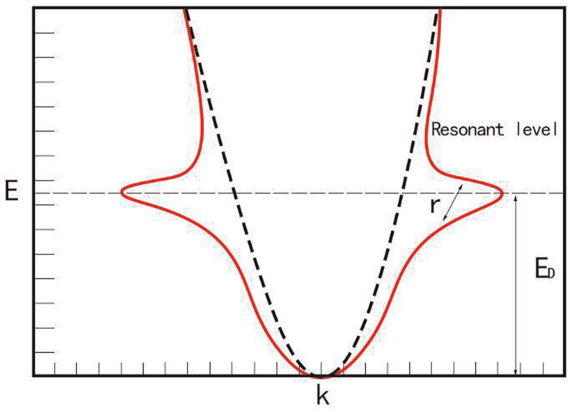

Figure 5.
Schematic view of the resonant level. Reproduced with permission from reference [25]. Copyright of The Royal Society of Chemistry 2012.

3.1.1.2 Energy band convergence

According to the relationship between the band degeneracy and density-of-states effective mass ($m_d^* = N_V^{2/3} m_b$), enhancement in density-of-states effective mass can also be realized by improving the band degeneracy. In principle, when there is no band extremum or the energy difference can be ignored in multiple bands, band degeneracy will increase. In addition, when multiple carrier pockets in the Brillouin zone degenerate, high band degeneracy can be obtained because they are symmetrically equivalent due to the symmetry of the crystal.

3.1.2 Carrier filtering effect

According to the Mott relation, the Seebeck coefficient can be expressed as [27].

$$S = \frac{-1}{e\sigma} \int \frac{\varepsilon - \mu}{T} \sigma(\varepsilon) \left[\frac{-\partial f^0(\varepsilon)}{\partial \boldsymbol{\varepsilon}} \right] \tag{35}$$

In Eq. (35), ε is the energy of the carrier, μ is the chemical potential, $\sigma(\varepsilon)$ is the differential conductivity, and $f^0(\varepsilon)$ is the Fermi distribution function. Furthermore, as can be seen from the equation, the contribution signs of charge carriers with energy less than the chemical potential and charge carriers with energy greater than the chemical potential to the Seebeck coefficient are opposite. As shown in **Figure 6**, low-energy electrons in n-type SiGe alloys have a negative impact on the Seebeck coefficient (green area). Therefore, the absolute value of the Seebeck coefficient decreases due to this negative effect [27]. Here, if preferential scattering on low-energy carriers (i.e., carrier filtering effect) can be achieved, the Seebeck coefficient can be improved [28]. Due to the fact that the carrier filtering effect essentially manipulates the carrier scattering mechanism, the scattering term in Eq. (34) indicates the enhancement of the Seebeck coefficient caused by the carrier filtering effect.

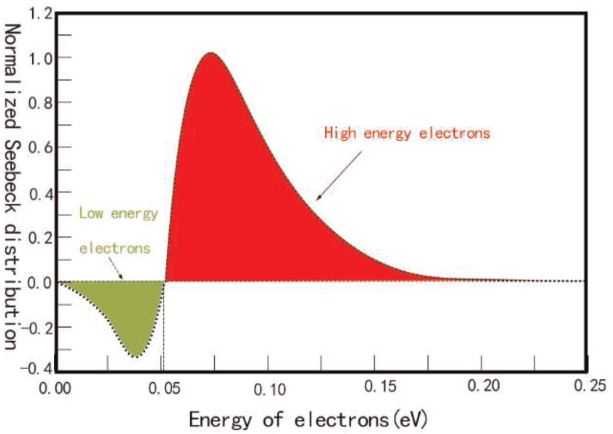

Figure 6.
Relationship between the energy of electrons and the normalized Seebeck distribution for heavily doped n-type SiGe alloy. Reproduced with permission from reference [28]. Copyright of The Royal Society of Chemistry 2009.

3.2 Mobility enhancement

In the case of elastic scattering, the carrier mobility of semiconductors with simple parabolic energy bands is [29].

$$\mu = \frac{e\langle\tau\rangle}{m^*} \tag{36}$$

where $\langle\tau\rangle$ is the average relaxation time and m^* is the effective mass. In simple terms, relaxation time can be regarded as a power function of carrier energy E, temperature T, and effective mass m^*, as shown below

$$\tau \propto E^r T^s m^{*t} \tag{37}$$

From Eqs. (36) and (37), it can be seen that the mobility depends on the band structure (i.e., m^*) and the carrier scattering mechanism (i.e., $\langle\tau\rangle$). Therefore, an effective strategy to improve carrier mobility is to regulate the effective mass and carrier scattering mechanism.

3.2.1 Effective mass engineering

Because the charge carriers are mainly scattered by acoustic phonons, Snyder pointed out that the nondegenerate mobility in multi-valley conduction can be expressed as [30].

$$\mu = \frac{2^{3/2}\pi^{1/2}\hbar^4 e C_1}{3m_I(m_b k_B T)^{3/2}\Xi^2} \tag{38}$$

where m_I is the inertial effective mass, C_1 is the composite elastic constant, and Ξ is the deformation potential coefficient. Hence, higher carrier mobility requires smaller band effective mass and inertial effective mass [30].

3.2.2 Manipulation of carrier scattering mechanism

When acoustic phonon waves propagate in a crystal, they cause compression and expansion of the local lattice. Therefore, it can cause disturbances in the band potential energy, leading to the scattering of charge carriers, known as acoustic phonon scattering [31]. Due to the constant existence of acoustic phonon scattering,

It can determine the upper limit of carrier mobility. Generally speaking, acoustic phonon scattering is one of the largest intrinsic scattering mechanisms in semiconductors, especially at high doping levels and high temperatures. According to Eq. (38), the deformation potential coefficient is a measure of the strength of electron-phonon interactions and a key parameter for evaluating thermoelectric performance. Low deformation potential coefficient of weak electron-phonon coupling leads to high carrier mobility [32–34]. However, the physical source of low deformation forces in materials is still unclear. The latest research indicates that the physical essence of low-strain materials is nonbonding orbitals that make significant contributions to electron transport [35].

3.2.3 Selecting doping sites

Based on the rigid band approximation, it is generally believed that dopants only change the Fermi level and carrier concentration. In the case of complete ionization of impurities, different dopants achieve the same effect. However, experiments have found that differences in dopants and doping sites may lead to variations in carrier mobility at high carrier concentrations.

The dopant does not alter the band structure to maintain the effectiveness of the rigid band approximation, which can be represented by the carrier concentration dependence of the Seebeck coefficient. Therefore, the difference in mobility should correspond to different measurements of scattering. Of course, there must be scattering of charge carriers by ionized impurities that generate charge carriers. However, when different dopants have the same valence, complete ionization, and random distribution, the ionization impurity scattering theory equivalently treats them. Therefore, different degrees of scattering should not be attributed to ionizing impurity scattering.

3.3 Carrier concentration optimization

The main thermoelectric parameters that determine the quality factor of thermoelectric materials are all related to carrier concentration and therefore heavily coupled with each other. It can be seen that the most effective strategy to improve thermoelectric performance is to optimize the carrier concentration. From a historical perspective, tuning of carrier concentration has been achieved through intentional introduction of exogenous impurities through chemical doping. In this way, the carrier concentration remains a constant value before bipolar conduction occurs, almost independent of temperature. However, the optimal carrier concentration (n_{opt}) is highly dependent on temperature, so thermoelectric performance is only optimized within a limited temperature range.

3.4 Phonon engineering

Given the relative independence of lattice thermal conductivity from other thermoelectric parameters, reducing lattice thermal conductivity is considered the most

direct means of improving thermoelectric performance. The dynamic theoretical expression for the thermal conductivity of three-dimensional materials is [36].

$$k(\Lambda) = \frac{1}{N_k} \sum_{k\lambda}^{\Lambda_{k\lambda} < \Lambda} \frac{1}{3} v_{k\lambda} \Lambda_{k\lambda} C_{vk\lambda} \tag{39}$$

where v, Λ, C_v are the phonon group velocity, phonon mean free path, and specific heat, respectively; λ labels a phonon band index (or branch), k refers to a point in the first Brillouin zone (with a k-point mesh), and N_k is the number of points. The mean free path of phonons is determined by multiple scattering mechanisms. Assuming that different scattering mechanisms are independent of each other, the Matthiessen's rule can be used to estimate the phonon mean free path.

$$\Lambda^{-1} = \sum \Lambda_i^{-1} \tag{40}$$

The latest progress in simulating phonon transport from scratch has greatly deepened our understanding of the thermal conduction mechanism of thermoelectric materials [37]. At the same time, the relationship between lattice thermal conductivity and material parameters was clarified. The low lattice thermal conductivity is attributed to the low sound velocity, large cell volume, long bond length (i.e., weak bonding), and large Grüneisen parameters (i.e., strong anharmonic).

3.4.1 Phonon-phonon scattering

The phonon-phonon interaction mechanism is that the first phonon causes periodic elastic strain (through anharmonic interaction), which adjusts the elastic constant of the crystal in space and time. The second phonon perceives the modulated elastic constant and scatters it, producing a third phonon, known as the three-phonon process [38].

3.4.1.1 Umklapp scattering

When the total momentum (K) of the phononic gas remains constant (K1 + K2 = K3), the three-phonon collision process is a normal process (or N-process). The phonon energy during the N process is only redistributed from the incident phonon to the excited phonon, without generating any thermal resistance. **Figure 7 (a)** and **(c)** indicate the presence of phonon net flow between the phonon source and phonon sink during the N process.

There is another case of three-phonon collision, which requires an additional reciprocal lattice vector (**G**) to maintain total momentum conservation ($K_1 + K_2 = K_3 + G$). This collision process is called the Umklapp process (or U process). Due to the fact that the wave vector K describing the phonon state can only be located in the first Brillouin zone, any wave vector K generated outside the first Brillouin zone during a collision must be moved to the first Brillouin zone by adding G (**Figure 7(d)**). This leads to net phonon backscattering during the U-process, resulting in thermal resistance (**Figure 7(b)**). Based on the physical mechanism of the U-process, the lattice thermal conductivity of materials can be limited at high temperatures, with a temperature dependence of $\kappa_{lat} \sim T^{-1}$.

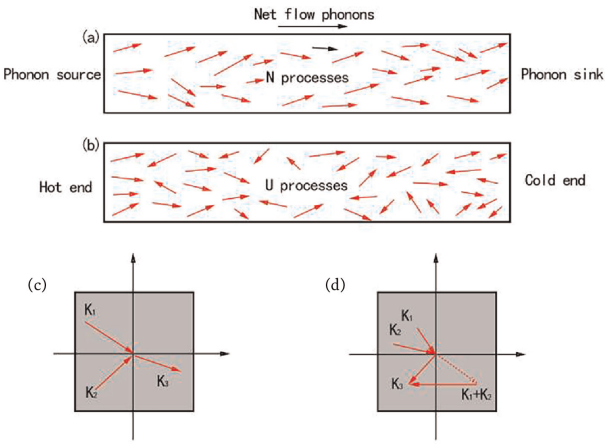

Figure 7.
N process (a) and U process (b) for the phonon gas. Phonon collision in a two-dimensional square lattice for (c) N process and (d) U process. Reproduced with permission from reference [38]. Copyright of 1976 by John Wiley & Sons, Inc.

3.4.1.2 Anharmonic effect

The theory of harmonic approximation may lead to some conclusions that are not consistent with reality: there is no thermal expansion (the equilibrium position of atoms does not depend on temperature), the force constant and elastic constant do not depend on temperature and pressure, the heat capacity at high temperatures is constant (Dulong Petit law), the isochoric heat capacity and isobaric heat capacity are equal ($C_V = C_p$), there is no interaction between phonons, the average free path and lifetime of phonons are infinite, and the thermal conductivity of harmonic crystals without impurities and defects is infinite; In the expansion of the potential energy of crystal atom interactions, terms of the third power and above are called non-harmonic terms. Many physical effects are caused by nonharmonic terms, such as vibration softening due to a decrease in the restoring force constant and scattering between phonons due to no longer independent vibration modes (phonons). Therefore, increasing the nonharmonic effect can be a beneficial strategy for limiting lattice thermal conductivity.

3.4.1.3 Acoustic and optical phonon coupling

Acoustic phonons: Low-frequency phonons formed by stimulated Brillouin scattering during the interaction between a light field and a medium. In acoustic mode, the crystal undergoes overall motion at a low frequency and can be regarded as a continuous medium elastic wave. Optical phonons: In crystals, atoms or ions vibrate around equilibrium positions, forming optical phonons. The frequency of optical mode is close to that of electromagnetic waves, making it easy to couple with electromagnetic fields. Acoustic phonons mainly contribute to lattice thermal conductivity due to their high group velocity. Based on the physical nature of the two types of phonons, significant thermal resistance can also be generated by mediating the coupling between optical phonons and acoustic phonons through relevant strategies.

3.4.1.4 Rattling modes

Phonon softening is an effective method to reduce lattice thermal conductivity. Designing lattice void structures filled with weakly bonded heavy atoms can significantly reduce lattice thermal conductivity, known as rattling modes. Slack and Tsoukala proposed the concept of phonon scattering for this type of rattling [39].

3.4.2 Phonon scattering by electrons

Acoustic phonon scattering is one of the important mechanisms of electron scattering. Due to the possible interaction between electrons and phonons, electron-phonon scattering is possible. Ziman was the first to study electron-phonon scattering [18]. Charge carriers are usually achieved through doping. As the impurity concentration increases, the wave functions of charge carriers overlap. When the overlap reaches a certain degree, it can be considered that the carriers are in a quasi-free state, forming an unfilled impurity band. The carriers in the band can collide with phonons and scatter phonons [40].

3.4.3 Scattering of phonons by microstructural defects

Figure 8 [41] shows that when the microstructure of solid materials contains point defects, dislocations, stacking faults, twin boundaries, grain boundaries, and nanostructures, it can distort the perfect crystal structure and hinder the propagation of phonons. The success of phonon engineering largely relies on shortening the phonon mean free path by introducing microstructural defects [41]. Based on different lattice environments and system temperatures, the average free path distribution of phonons ranges from a few angstroms to several hundred nanometers. The effective scattering of phonons of different wavelengths requires the design of defects with corresponding characteristic sizes [42–44]. Phonon scattering based on manipulating microstructural defects has been extensively studied and proven to be highly effective in minimizing lattice thermal conductivity and improving thermoelectric performance.

3.4.3.1 Phonon scattering by point defects

Point defects such as dopants, alloy atoms, isotopes, vacancies, and gaps can effectively scatter high-frequency phonons due to their smaller characteristic sizes. When the phonon wavelength is greater than the size of the point defect, the point defect will strongly scatter phonons. Without considering resonance or multiple scattering effects, the phonon relaxation time $\langle\tau\rangle$ is related to the phonon frequency ω [45, 46].

$$\frac{1}{\tau_{PD}} = \phi c^2 \omega^2 \tag{41}$$

Where ϕ is the fractional concentration of point defects, and c is a contrast parameter such as mass or strain.

Atomic defects contribute to perturbation energy in three ways: (a) changes in kinetic energy due to differences in mass; (b) Potential energy generated by changes in the elastic constants of atomic bonds; (c) Potential energy caused by an elastic strain field that changes the elastic constants of atomic bonds [47, 48]. Callaway [49, 50], Klemens [51], and Abeles [48, 52] reported a theoretical study on the effect of point defects on lattice thermal conductivity.

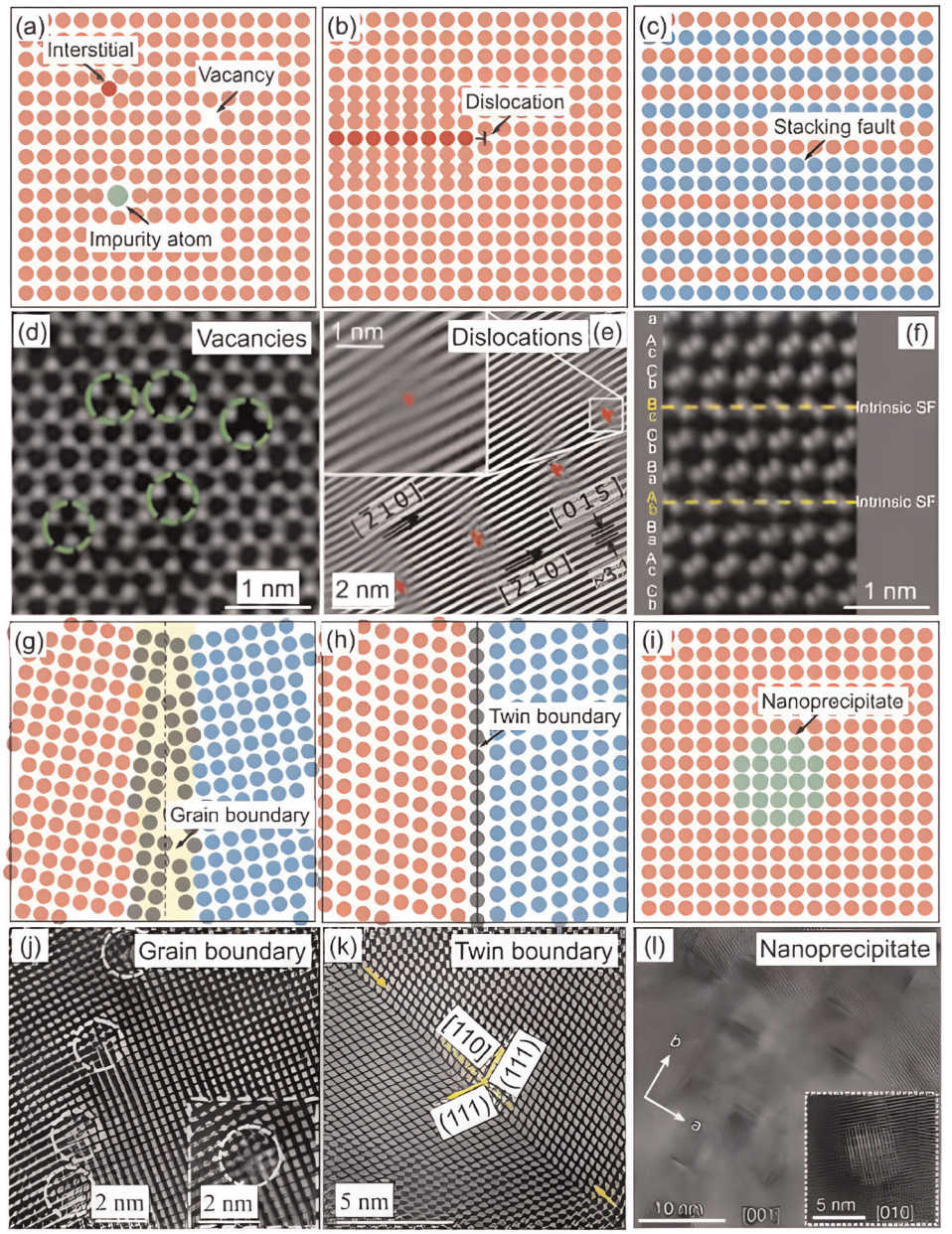

Figure 8.
Schematic views for (a) point defects, (b) dislocation, (c) stacking fault, (g) grain boundary, (h) twin boundary, and (i) nanoprecipitates. The rest of panels are the corresponding TEM images for the microstructural defect. Reproduced with permission from reference [41]. Copyright of 2018 Materials Research Society.

3.4.3.2 Phonon scattering by grain boundaries

For infinite lattices, the thermal resistance of insulating crystals rapidly decreases with decreasing temperature [53]. When the temperature of a given crystal with a finite size is below its corresponding critical temperature, its phonon free path is the

size of the crystal. Once this situation occurs, the scattering of phonons by crystal boundaries will generate additional resistance [54]. The Casimir theory [54] provides the diffuse reflection of phonons from sample boundaries as the primary mechanism for achieving phonon equilibrium at very low temperatures. The relaxation time of boundary scattering can be expressed as

$$\frac{1}{\tau_{GB}} = \frac{v}{L} \tag{42}$$

where L is the average dimension of the sample.

3.4.3.3 Phonon scattering by dislocations

Dislocations are composed of dislocation lines and dislocation nuclei, and the crystal structure near the dislocation line is a finite strain, so phonons will be scattered when passing near the dislocation. The scattering degree of phonons by dislocation cores is much higher than that of phonons by dislocation stress fields. Dislocations can also move under the influence of phonons, and when dislocation oscillations occur, phonons will be re-emitted [55]. Klemens pointed out that both the type of dislocation and the dislocation line scatter phonons in the direction of the temperature gradient. The relaxation time of scattered phonons from dislocation lines perpendicular to the temperature gradient is [47].

$$\frac{1}{\tau_{D,line}} = C_1 \frac{b^2}{a^2} \omega \tag{43}$$

In Eq. (43), C_1 is a constant, b is the magnitude of the Burgers vector, and a is the lattice parameter. The relaxation time of phonon scattering by dislocation nuclei is expressed as

$$\frac{1}{\tau_{D,core}} = C_2 a^2 \omega^3 \left(\frac{\Delta M}{M}\right)^2 \tag{44}$$

where C_2 is a constant, M is the atomic mass of the unit cell, and ΔM is the mass difference.

3.4.3.4 Scattering of phonons by nanoparticles

In the synthesis process of bulk materials, nanoparticles and nanoprecipitate-embedded structures can be obtained through synergistic modulation of processes and components to reduce the thermal conductivity of the material. A. Shakouri provided the relaxation of phonon scattering by nanoparticles as [56].

$$\frac{1}{\tau_{NP}} = v\left(\sigma_s^{-1} + \sigma_1^{-1}\right)^{-1} \rho \tag{45}$$

$$\sigma_s = 2\pi R^2 \tag{46}$$

$$\sigma_1 = \pi R^2 \frac{4}{9} \left(\frac{\Delta D}{D}\right)^2 \left(\frac{\omega R}{v}\right)^4 \tag{47}$$

Where ρ and R are the density and radius of nanoparticles, respectively, and D and ΔD are the density of the matrix material and the density difference between nanoparticles and matrix material, respectively.

In summary, various modulations of material microstructures can be obtained by modulating atomic and molecular structures, creating nanostructures and multi-scale structures in TE materials to optimize electron and phonon transport. Various modulation methods can improve material properties, but the performance improvement is limited, and all methods also lack universality. In addition, all the material performance optimization strategies mentioned above are independently applied to phonon and electron transport. The actual situation is that the transport of electrons and phonons in materials is inseparable and permanently coupled. Therefore, exploring the optimized coupling of electrons and phonons to significantly improve the performance of thermoelectric materials may be an effective strategy and a good paradigm to break through the upper limit of the coefficient of merit of thermoelectric materials.

4. Physical paradigm for synergistically reducing the thermal conductivity and improving the power factor

According to the definition of the TE quality factor, high ZT values originate from material systems with high conductivity, a large Seebeck coefficient, and low thermal conductivity. In the past few decades, traditional methods for optimizing TE performance have relied on electron-phonon transport separation, electronic band engineering, and phonon scattering mechanism modulation. However, even at various optimization levels, only moderate ZT values can usually be obtained. This section explores the physical paradigm of synergistic electro/phonon transport based on the mechanism of electron-phonon interaction, starting from the phonon drag effect and superconducting BCS theory.

4.1 BCS theory overview

Experimental measurements of the electromagnetic properties of superconductors tell us that the charge of charge carriers in superconductors is twice that of electrons, implying that electrons always pair up. Secondly, superconductors can theoretically be effectively described by a "macroscopic wave function," which is a characteristic of boson systems at low temperatures. A composite particle composed of two fermions (spin half integer) has an integer spin, while a boson has an integer spin. It seems that a composite particle composed of two fermions is a boson. But in fact, this understanding is naive: the analysis under the second quantization system denies this point; however, the paired two fermions are somewhat similar to bosons, and superconductors do indeed exhibit Cooper pair condensation (BEC) at low temperatures, similar to boson condensation.

The measurement of the specific heat of superconductors at low temperatures tells us that superconductivity has an energy gap—to restore the superconducting state to normal through heating, a certain energy gap needs to be overcome, just like the existence of an energy gap in a semiconductor/insulator; the latter is non-conductive and does not match the conductivity of superconductors. Therefore, based on the above situation, a mechanism is needed to change the electronic system originally distributed to the Fermi surface at low temperatures so that some electrons pair up to

form approximate bosons and form macroscopic condensation. At the same time, there should be an energy gap between the condensed paired electrons and the normal electron states to maintain this state and prevent it from being easily destroyed by external energy such as heating.

Bardeen, Cooper, and Schrieffer, three physicists, presented their superconducting theory: based on the interaction between electrons and phonons, they reasonably explained the above phenomenon.

Electron-phonon interaction can lead to effective attraction between electrons. Phonons indicate that the atomic nucleus has deviated from its equilibrium position, and the displacement can be represented by the phonon generation/annihilation operator:

$$\overrightarrow{u_i} = \sum\nolimits_{\vec{q}} \left(\frac{\hbar}{2M\omega_{\vec{q}}} \right)^{1/2} \left(\hat{a}^{\dagger}_{\vec{q}} + \hat{a}_{-\vec{q}} \right) e^{i\vec{q}\overrightarrow{R_i}} \tag{48}$$

Where $\vec{q}$ represents the momentum of phonons in momentum space.

The change in potential energy generated by a small deviation of the atomic nucleus is

$$\delta V_{tot} = \sum\nolimits_i \frac{\partial V\left(\overrightarrow{x_e} - \overrightarrow{R_i}\right)}{\partial R_i} \bullet \overrightarrow{u_i} \tag{49}$$

The Hamiltonian of electron-phonon interaction is

$$\hat{H}_{el-ph} = V_{tot} + \delta V_{tot} \tag{50}$$

In order to obtain an effective theory of the interaction between electrons, the path integral/partition function of the electron field and phonon field (coupling) can be considered, and the phonon field can be directly integrated to obtain the part where only electrons remain; it is also possible to simply consider the scattering of electrons and phonons—represented by Feynman diagrams (**Figure 9**). Just as exchanging photons between electrons creates an effective interaction potential—Coulomb

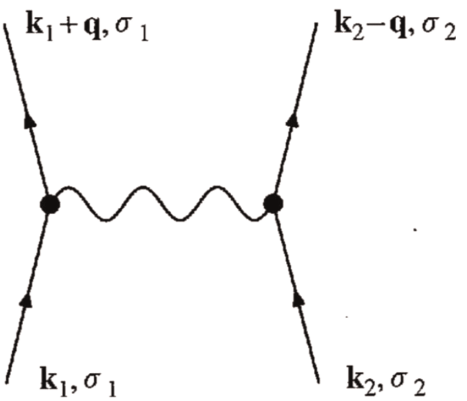

Figure 9.
Interaction of fermions via exchange of a boson.

potential—exchanging phonons between electrons also creates an effective potential energy.

Obtain the indirect interaction potential between electrons caused by phonons, which in momentum space is

$$V_{eff}\left(\vec{q},\vec{k}\right)=\left|g_{\vec{q}}\right|^{2}\frac{\hbar\omega_{\vec{q}}}{\left(\epsilon_{\vec{k}}-\epsilon_{\vec{k}+\vec{q}}\right)^{2}-\left(\hbar\omega_{\vec{q}}\right)^{2}} \tag{51}$$

When $\left|\epsilon_{\vec{k}}-\epsilon_{\vec{k}+\vec{q}}\right|<\omega_{\vec{q}}$, the sign of $V_{eff}\left(\vec{q},\vec{k}\right)$ is negative, which means an attractive force.

4.2 Phonon drag effect

Phonon drag effect refers to the fluctuation of crystal atomic density caused by the propagation of sound waves (longitudinal waves) in a crystal, forming additional potential field waves with the same period as the sound waves. In semiconductors, this potential field wave manifests as a small distorted periodic potential field; in piezoelectric semiconductors, it manifests as a large periodic piezoelectric potential field. Sound waves are essentially long acoustic waves of lattice vibration quantized into phonons, and the resulting potential field waves can be seen as the effect of phonons—phonon potential field waves.

When the average free path of an electron is less than the wavelength of the acoustic wave, the electron will be frequently scattered by phonons and captured by the valley of the phonon potential field wave. At this point, as the sound wave valley, electrons are dragged by the phonon potential field wave, resulting in the phonon drag effect, as shown in **Figure 10**. The phonon potential field in piezoelectric semiconductors has a larger amplitude, leading to a more significant traction effect. Ultrasonic waves can also generate a larger amplitude periodic potential field, thereby enhancing the drag effect on electrons.

The phonon drag effect causes an uneven distribution of electrons in semiconductors, where electrons are pulled forward by phonons, which inevitably leads to a greater concentration of electrons to one side, resulting in the generation of an electromotive

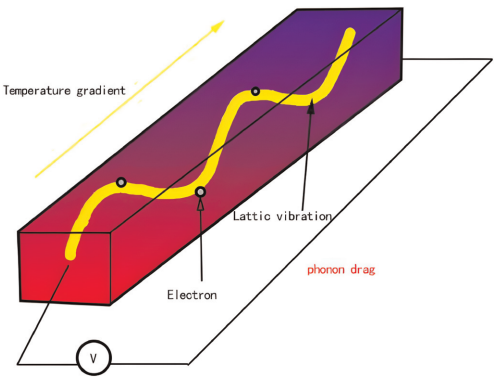

Figure 10.
Schematic diagram of phonon drag effect.

force. When an electric field acts on electrons, causing them to accelerate, the phonon drag effect should affect the propagation of sound waves. When the electron drift velocity is greater than the sound wave velocity, the electron pushes the phonon potential field wave, which enhances the sound wave energy and forms the basis of the ultrasonic amplifier. On the contrary, when the drift velocity of electrons is lower than that of sound waves, the energy of sound waves is transferred to electrons, resulting in a decrease in the amplitude of sound waves, that is, sound wave attenuation.

4.2.1 Non-diffusive thermoelectric transport caused by phonons (similar effects can also occur with magnons/spin waves)

Consider testing the Seebeck coefficient: apply a temperature gradient to the solid and measure the potential difference under an open circuit. The lattice waves generated by lattice vibrations have a certain frequency spectrum and propagate at a certain speed in the crystal. During the propagation process, thermal energy can be carried from the hot end to the cold end, resulting in a non-uniform distribution of phonons. This means that the scattering rate of charge carriers traveling along the temperature gradient is not equal to the scattering rate of charge carriers traveling in the opposite direction, resulting in a net current in the direction of the temperature gradient. However, the actual open circuit state cannot maintain charge flow, so the system has to establish a finite electric field to compensate for the excess scattering experienced by charge carriers traveling in one of the two directions. The additional electric field generated is the contribution of phonon drag to the Seebeck coefficient, in addition to the electron diffusion response.

Consider the Peltier test: measure the ratio of energy flow to current along the sample without any temperature gradient. There is a net current along the sample, which causes the scattering rates of electrons and phonons moving in each other's direction to be different from those in the opposite direction. As a result, the phonon distribution is no longer balanced, ultimately producing an additional energy flow in addition to the energy flow purely brought by electrons, which is the contribution of phonon drag to the Peltier coefficient.

4.2.2 Phonon drag theory in semiconductors (Herring theory)

For semiconductors, phonon drag is quantitatively described from the perspective of phonons. Herring equates the rate at which a phonon system gains crystal momentum from electrons with the rate at which it loses crystal momentum through U-processes and boundary scattering [57].

$$\left.\frac{d\mathbf{P}}{dt}\right|_e = f^{el.} ne\mathbf{E} \tag{52}$$

Here, P is the crystal momentum per unit volume, $f^{el.}$ is the proportion of electron momentum loss (with a value of 1 in the absence of impurity scattering), and $ne\mathbf{E}$ is the force per unit volume, where $\mathbf{E}$ is the electric field and n is the carrier concentration.

Assuming the relaxation time of electron-phonon scattering is τ_{ph-e}, we have

$$\left.\frac{d\mathbf{P}}{dt}\right|_e = \frac{\mathbf{P}}{\tau_{ph-e}} \tag{53}$$

The energy flux density j_q caused by crystal momentum is

$$\mathbf{J}_q = \mathbf{P}\overline{v}_s^2 \tag{54}$$

Where $\overline{v}_s$ is the average speed of sound, so

$$\mathbf{J}_q = \overline{v}_s^2 \tau_{ph-e} f^{el.} ne\mathbf{E} = \overline{v}_s^2 \tau_{ph-e} f^{el.} \frac{\mathbf{J}_e}{\mu} \tag{55}$$

Based on Eq. (6), the contribution of phonon drag to the Peltier coefficient is

$$\Pi_g = f^{el.} \frac{\overline{v}_s^2 \tau_{ph-e}}{\mu} \tag{56}$$

By using the Kelvin relationship, the thermoelectric potential generated by phonon drag can be obtained as

$$\mathrm{S}_g = \frac{1}{T} f^{el.} \frac{\overline{v}_s^2 \tau_{ph-e}}{\mu} \tag{57}$$

The Herring scene discussed above has many simplifications. Electron-phonon coupling is viewed from the perspective of phonons, and their flow carries energy as a simple reaction to their collision with electrons.

4.3 A new paradigm for enhancing thermoelectric quality factors

4.3.1 Discussion on the mechanism of electron-phonon interaction for improving the performance of thermoelectric materials

In recent decades, the improvement of thermoelectric material performance in the scientific community has been based on the strategy of electron crystal-phonon glass. The specific implementation strategy is mostly to design various methods to decouple the correlation between electron and phonon transport. However, the actual performance improvement is limited. Although some material systems are based on modulation mechanisms that can greatly improve material performance, the stability of materials during thermoelectric operation has not been fully verified.

The most concerned thermoelectric semiconductor material in the industry at present is undoubtedly bismuth telluride polar semiconductor. Fröhlich interaction is an interaction between electrons and longitudinal optical phonons (LO phonons) in polar semiconductor materials. This interaction generates a macroscopic electric field, leading to long-range coupling between electrons and phonons, forming a quasiparticle called a polaron. The strength of Fröhlich interaction is measured by a dimensionless Frohlich coupling constant. In polarized semiconductors, due to the coupling between polarons and LO phonons, charge carriers transfer their initial kinetic energy to the lattice through a highly efficient relaxation mechanism.

According to Eqs. (1, 2), the thermal conductivity (open circuit), κ, under zero current conditions and the thermal conductivity (short circuit) under zero potential gradient can be obtained as follows:

$$\kappa|_{J_e=0} = \frac{1}{T^2} \frac{L_{11}L_{22} - L_{12}L_{21}}{L_{11}} \tag{58}$$

$$\kappa'|_{E=0} = \frac{1}{T^2} L_{22} \tag{59}$$

By using Eqs. (8–10) and defining thermal inducing electric conductivity as $\alpha = \frac{e}{T^2} L_{12}$, we can obtain

$$\kappa' = \kappa\left(1 + \frac{\alpha^2 T}{\sigma\kappa}\right) \tag{60}$$

Where $\frac{\alpha^2 T}{\sigma\kappa}$ is the thermoelectric figure of merit. Increasing thermal-induced electric conductivity can improve thermoelectric figure of merit (constructing an optimization strategy based on Eq. (32)). This also provides a new perspective for the design of high-performance thermoelectric materials.

Based on BCS theory and the phonon drag effect, we can design a multi-element thermoelectric structure material with uniformly distributed nanocrystals. However, one should always keep in mind that the presence of nanoinclusions might adversely affect the conducting carriers. To achieve this, we must face the following issues:

Firstly, the design of nanostructures is based on the preferential scattering of phonons carrying heat while maintaining the integrity of the charge carrier transport path. In order to match the band structure of carrier transport, nanoinclusions or nanoscale defects must have only a small band edge offset relative to the band edge of the matrix [58]. In n-type nanocomposites, the conduction band edges of the nanoinclusions and matrix should be closely matched, with an energy difference generally not exceeding a few $k_B T$, to minimize electron scattering at the interface potential barrier. Experimental and theoretical studies have shown that the interface and boundary morphology in nanostructured materials should meet the requirement of atomic coherence or alignment at very small angles to maintain high carrier mobility [59].

Secondly, based on Eq. (51) in BCS theory, phonon exchange can achieve the attractive potential energy of electrons, thereby optimizing carrier transport. The open questions are how to modulate the electron distribution near the Fermi surface and ensure that the energy change of electrons after exchanging phonons is less than the corresponding phonon energy.

Thirdly, design material structures based on the phonon drag effect to achieve efficient coupling between long wave acoustic phonons and electrons. The open questions are how to achieve effective transfer of electron-phonon momentum and large electron-phonon interaction relaxation time.

Fourthly, the calculation of interface phonon modes and the revelation of the interaction mechanism between interface phonons and electrons. Nano-embedded materials or bulk materials containing nano-inclusions inevitably contain a large number of grain boundaries, and interface phonon modes will inevitably affect electron transport and energy exchange. A deep understanding of the interaction mechanism between interface phonon modes and electrons is the basis for constructing high-performance thermoelectric materials.

Fifthly, constructing nanostructured phononic metamaterials and exploring the quantitative relationship between phonon fluctuations and particle effects on thermal conductivity in phononic metamaterials. Research on the modulation mechanism of thermal conductivity by local resonance hybridization based on phonon fluctuation, and obtain the physical basis for synergistic regulation of phonon fluctuation and particle transport.

4.3.2 Electron-phonon coupling mechanism and its strategy in optimizing the properties of thermoelectric materials

Nanostructured materials have achieved great success. The basic strategy is to decouple the correlation between electrons and phonons and introduce clusters or microstructures that generate multiple scattering to phonons to reduce material thermal conductivity, but they are gradually running out of power in further reducing thermal conductivity, and the lattice deformation potential caused by lattice vibration always interacts with electrons. It is becoming increasingly evident that any further benefits of ZT must now come from improvements in power factor. The current research on improving power factor aims to identify materials with good band structure characteristics, such as resonance states and low-dimensional "class" features in bulk materials, or band structure engineering, such as band convergence strategies. In fact, most promising TE materials have complex band structures with multiple energy valleys and bands that extend throughout the entire Brillouin zone (BZ). In summary, instead of forcibly decoupling the electron-phonon correlation, it is more advantageous to use a new paradigm of electron-phonon correlation to optimize the key properties of thermoelectric materials. Of course, it is computationally challenging to utilize the entire phonon and electron dispersions for full transport calculations; thus, it is common to employ reasonable approximations.

In periodic solids, the electron-phonon coupling effect is usually discussed in terms of the Hamiltonian [60].

$$\hat{H} = \hat{H}_e + \hat{H}_{ph} + \hat{H}_{e-ph} \tag{61}$$

Based on the Fock space, the generation annihilation operator can be established, and the Hamiltonian of fermions can be obtained as

$$\hat{H}_e = \sum_{nk} \varepsilon_{nk} \hat{c}^{\dagger}_{nk} \hat{c}_{nk} \tag{62}$$

describes noninteracting quasiparticles with crystalline momentum **k**, band index n, and dispersion $\varepsilon_{n\mathbf{k}}$, while

$$\hat{H}_{ph} = \sum_{q\nu} \omega_{q\nu} \left(\hat{a}^{\dagger}_{q\nu} \hat{a}_{q\nu} + \frac{1}{2} \right) \tag{63}$$

is the Hamiltonian associated with noninteracting phonons with wave vector q, mode index ν, and frequency $\omega_{q\nu}$.$\hat{c}^{\dagger}_{nk}$ and $\hat{c}_{nk}$ ($\hat{a}^{\dagger}_{q\nu}$ and $\hat{a}_{q\nu}$) are fermionic (bosonic) creation and annihilation operators. Finally,

$$\hat{H}_{e-ph} = \frac{1}{\sqrt{N_p}} \sum_{\substack{k,q \\ mn\nu}} g_{mn\nu}(k,q) \hat{c}^{\dagger}_{mk+q} \hat{c}_{nk} \left(\hat{a}_{q\nu} + \hat{a}^{\dagger}_{-q\nu} \right) \tag{64}$$

Described the first-order coupling of atomic displacement, where N_p is the number of unit cells in the Born von Karman supercell, and $g_{mn\nu}(k,q)$ is the element of the e-ph coupling matrix. In principle, Eq. (61) should include the so-called Debye Waller

(DW) Hamiltonian, which gives the second-order coupling of atomic displacement [60]. This term makes a significant contribution to the real part of self-energy (SE) and therefore must be included when calculating quasi-particle correction and temperature-dependent band structures. However, we will mainly focus on the imaginary part of e-ph SE, so the DW term will be ignored [60].

The relationship between the multibody Hamiltonian in Eq. (61) and density functional theory (DFT) was established by using the Kohn Sham (KS) band structure in Eq. (62) and the phonons in density functional perturbation theory (DFPT) in Eq. (63) [60]. Finally, the e-ph matrix element, $g_{mnv}(k,q)$, is computed using

$$g_{mnv}(k,q) = <\psi_{mk+q}|\Delta_{q\nu}V^{KS}|\psi_{nk}> \tag{65}$$

where ψ_{nk} is the KS Bloch state and $\Delta_{q\nu}V^{KS}$ is the first-order variation of the self-consistent KS potential,

$$\Delta_{q\nu}V^{KS} = \frac{1}{\sqrt{2\omega_{q\nu}}}\sum_{p\kappa\alpha}\frac{\partial V^{KS}}{\partial \Gamma_{\kappa\alpha}}\frac{e_{\kappa\alpha,\nu}(q)}{\sqrt{M_\kappa}}e^{i_q * R_p} \tag{66}$$

where $e_{\kappa\alpha,\nu}(q)$ is the α-th Cartesian component of the phonon eigenvector for the atom κ in the unit cell, M_κ its atomic mass, R_p are lattice vectors identifying the unit cell p,and τ_k the ion position in the unit cell. Following the convention of Ref. [60], V^{KS} consists of contributions from the Hartree part (V^H), the exchange-correlation (XC) potential (V^{xc}), and the bare pseudopotential term that, in turn, consists of the local (V^{loc}) and nonlocal (V^{nl}) parts. We can write Eq. (66) in terms of a lattice-periodic function $\Delta_{q\nu}V^{KS}$ defined as:

$$\Delta_{q\nu}V^{KS} = e^{i\mathbf{qr}}\Delta_{q\nu}v^{KS} \tag{67}$$

where,

$$\Delta_{q\nu}v^{KS} = \frac{1}{\sqrt{2\omega_{q\nu}}}\sum_{\kappa\alpha}\frac{e_{\kappa\alpha,\nu}(q)}{\sqrt{M_K}}\partial_{\kappa\alpha,q}v^{KS} \tag{68}$$

and,

$$\partial_{\kappa\alpha,q}v^{KS} = \sum_p e^{-i\mathbf{q}(\mathbf{r}-\mathbf{R_p})}\left.\frac{\partial V^{KS}}{\partial \Gamma_{\kappa\alpha}}\right|_{(\mathbf{r}-\mathbf{R_p})} \tag{69}$$

It is the first derivative of the KS potential (Kohn Sham single electron interaction potential), which can be obtained by self-consistently solving the Sternheimer equation system using DFPT under a given $(\kappa\alpha, q)$ perturbation [61].

According to the theoretical description of e-ph interactions mentioned above, e-ph interactions can modulate the transport characteristics of electrons. The electron lifetime due to the e-ph interactions is related to the inverse of the imaginary part of the e-ph Fan-Migdal SE (energy level correction under the interaction of electrons and phonons) [60]; the diagonal matrix elements of the SE in the KS basis set are given by

$$\sum_{nk}^{FM}(\omega,\varepsilon_F,T)=\sum_{m,\nu}\int_{BZ}\frac{dq}{\Omega_{BZ}}\left|g_{mn\nu}(k,q)\right|^2 \times\left[\frac{n_{q\nu}(T)+f_{mk+q}(\varepsilon_F,T)}{\omega-\varepsilon_{mk+q}+\omega_{q\nu}+i\eta}+\frac{n_{q\nu}(T)+1-f_{mk+q}(\varepsilon_F,T)}{\omega-\varepsilon_{mk+q}-\omega_{q\nu}+i\eta}\right] \tag{70}$$

where $f_{mk+q}(\varepsilon_F,T)$ and $n_{q\nu}(T)$ correspond to the Fermi-Dirac and Bose-Einstein occupation functions at temperature T and ε_F is the Fermi level. For simplicity, the temperature and Fermi level are directly considered as parameters. The integral in Eq. (70) is performed over the q points in the BZ of volume Ω_{BZ}, and η is a positive real infinitesimal.

In the $\eta\rightarrow 0^+$ limit, the imaginary part of the SE (Eq. (70)) is evaluated at the KS energy given by [60].

$$\lim_{\eta\rightarrow 0^+}\Im\left\{\sum_{nk}^{FM}(\varepsilon_{nk})\right\}=\pi\sum_{m,\nu}\int_{BZ}\frac{dq}{\Omega_{BZ}}\left|g_{mn\nu}(k,q)\right|^2 \times[(n_{q\nu}+f_{mk+q})\delta(\varepsilon_{nk}-\varepsilon_{mk+q}+\omega_{q\nu}) +(n_{q\nu}+1-f_{mk+q})\delta(\varepsilon_{nk}-\varepsilon_{mk+q}-\omega_{q\nu}] \tag{71}$$

and corresponds to the linewidth of the electron state *nk* due to the scattering with phonons. Finally, the electron lifetime τ_{nk} is inversely proportional to the linewidth of the SE evaluated at the KS energy [62]:

$$\frac{1}{\tau_{nk}}=2\lim_{\eta\rightarrow 0^+}\Im\left\{\sum\nolimits_{nk}^{FM}(\varepsilon_{nk})\right\} \tag{72}$$

Based on the relaxation time approximation of the linear Boltzmann equation, the generalized transport coefficient can be expressed as:

$$L_{\alpha\beta}^{(m)}=-\sum_n\int\frac{dk}{\Omega_{BZ}}v_{nk,\alpha}v_{nk,\beta}\tau_{nk} \times(\varepsilon_{nk}-\varepsilon_F)^m\left.\frac{\partial f}{\partial\varepsilon}\right|_{\varepsilon_{nk}} \tag{73}$$

where $v_{nk,\alpha}$ is the $\alpha-th$ component of the matrix element v_{nk} of the electron velocity operator. Using the commutator of the Hamiltonian with the position operator, we can take v_{nk} as: [63].

$$v_{nk}=\frac{\partial\varepsilon_{nk}}{\partial k}=<\psi_{nk}|\hat{p}+i[V^{nl},r]|\psi_{nk}> \tag{74}$$

Among them, $\hat{p}$ is the momentum operator, as done in the DFPT calculation of the response to external electric fields [64]. The group velocity can be used to calculate the transport lifetime within the so-called momentum relaxation time approximation [65].

According to Eq. (70), the effective **k** and **q** points that determine the electron-phonon interaction can be obtained as shown in **Figure 11** (a) **k** and (b) **q** points for the computation of the SE in the case of a single parabolic conduction band at the Γ

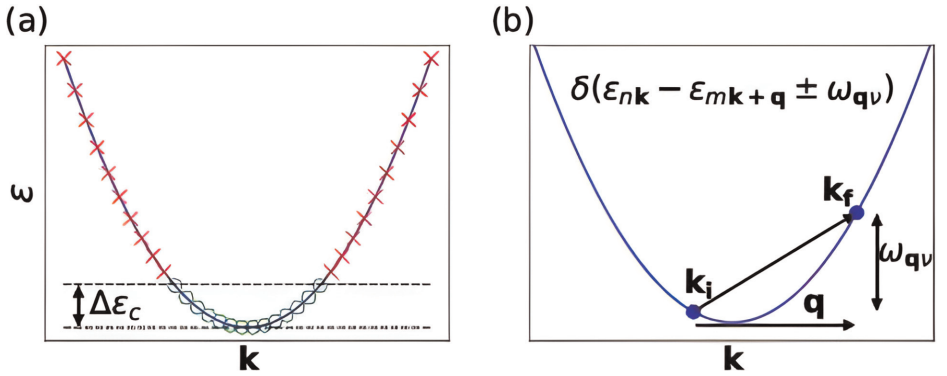

Figure 11.
(a) **k** *and (b)* **q** *points for the computation of the SE in the case of a single parabolic conduction band at the* Γ *point.*

point. (a) States represented by green dots (red crosses) are included (excluded) in (from) the transport computation according to the input variable $\Delta\varepsilon_c$. (b) For initial and final electron states $\mathbf{k_i}$ and $\mathbf{k_f}$, the wave vector $\mathbf{q} = \mathbf{k_f} - \mathbf{k_i}$ requires a phonon mode with frequency $\omega_{q\nu} = \varepsilon_{kf} - \varepsilon_{ki}$. If this condition is not fulfilled, the **q** point is ignored.

In the case of a determined composition, the thermal conductivity of a material is mainly determined by its thermal diffusivity and essentially by its bonding state. Based on the long-range coupling effect of electron-phonon, on the one hand, it can reduce short-range forces to soften phonon modes, and on the other hand, it can smooth out the lattice potential energy field that determines the electronic state and promote electron transport, simultaneously achieving energy filtering of electrons. Based on the hierarchical nanostructure design strategy, the electron-phonon coupling probability that is conducive to enhancing the thermoelectric effect is selected. Directed high-momentum electronic states are obtained by absorbing phonons, while small-momentum electronic states are filtered by emitting phonons. In addition, the phonon softening mechanism of the nanostructure is used to reduce the directional thermal conductivity of phonons and the adverse scattering of diffused electrons. Abnormal changes in the Debye-Waller factor can reflect the lattice softening phenomenon. In a normal electronic system, the electron-phonon interaction weakens the persistent current through the Debye-Waller factor, indicating that this factor can serve as an indirect indicator of the coupling strength between electrons and lattice vibrations. Finally, in a quantum well, an external electromagnetic field regulates the electron-phonon interaction, further affecting the polaron correction energy, which is also related to the correction of the Debye Waller factor.

5. Conclusion

This chapter starts from the basic theory of thermoelectricity and introduces the thermoelectric transport equation and the Boltzmann transport equation that controls phonon and electron transport. Subsequently, various innovative strategies for optimizing thermoelectric materials in recent decades were reviewed, and the related progress was evaluated. Finally, based on the superconducting BCS theory and phonon drag effect, this chapter proposes a new physical paradigm different from the

phonon-glass-electron-crystal method. The core of the new paradigm is to shift from decoupling the electron-phonon transport process to optimizing the electron-phonon coupling mechanism and provides a theoretical mechanism for improving the performance of thermoelectric materials by optimizing the electron-phonon coupling. Identified the material design concepts and challenges for implementing the new paradigm.

Conflict of interest

The authors declare no conflict of interest.

Author details

Hong Liu* and Xinli Cheng
School of Physics and Technology, Suzhou University of Science and Technology, Suzhou, China

*Address all correspondence to: hliu@usts.edu.cn

References

[1] Snyder GJ, Toberer ES. Complex thermoelectric materials. Nature Materials. 2008;**7**:105-114

[2] Sootsman JR, Chung DY, Kanatzidis MG. New and old concepts in thermoelectric materials. Angewandte Chemie-International Edition. 2009;**48**: 8616-8639

[3] Zhu T, Liu Y, Fu C, Heremans JP, Snyder JG, Zhao X. Compromise and synergy in high-efficiency thermoelectric materials. Advanced Materials. 2017;**29**:1605884

[4] Heremans JP, Jovovic V, Toberer ES, Saramat A, Kurosaki K, Charoenphakdee A, et al. Enhancement of thermoelectric efficiency in PbTe by distortion of the electronic density of states. Science. 2008;**321**:554-557

[5] Pei Y, Shi X, LaLonde A, Wang H, Chen L, Snyder GJ. Convergence of electronic bands for high performance bulk thermoelectrics. Nature. 2011;**473**: 66-69

[6] Liu H, Shi X, Xu F, Zhang L, Zhang W, Chen L, et al. Copper ion liquid-like thermoelectrics. Nature Materials. 2012; **11**:422-425

[7] Liu R, Chen H, Zhao K, Qin Y, Jiang B, Zhang T, et al. Entropy as a gene-like performance indicator promoting thermoelectric materials. Advanced Materials. 2017;**29**:1702712

[8] Zhao LD, Lo SH, Zhang Y, Sun H, Tan G, Uher C, et al. Ultralow thermal conductivity and high thermoelectric figure of merit in SnSe crystals. Nature. 2014;**508**:373-377

[9] Pei YL, Wu HJ, Wu D, Zheng FS, He JQ. High thermoelectric performance realized in a BiCuSeO system by improving carrier mobility through 3D modulation doping. Journal of the American Chemical Society. 2014;**136**: 13902-13908

[10] Muchler L, Casper F, Yan B, Chadov S, Felser C. Topological insulators and thermoelectric materials. Physica Status Solidi RRL: Rapid Research Letters. 2013; **7**:91-100

[11] Uchida K, Takahashi S, Harii K, Ieda J, Koshibae W, Ando K, et al. Observation of the spin Seebeck effect. Nature. 2008;**455**:778-781

[12] Chen G. Nanoscale Energy Transport and Conversion: A Parallel Treatment of Electrons, Molecules, Phonons, and Photons. London: Oxford University Press; 2005

[13] Ashcroft NW, Mermin ND. Solid State Physics. Holt; 1976

[14] Nolas GS, Sharp J, Goldsmid HJ. Thermoelectrics: Basic Principles and New Materials Developments. Berlin: Springer; 2001

[15] Ziman JM. Electrons and Phonons: The Theory of Transport Phenomena in Solids. London: Clarendon Press; 1960

[16] Lindsay L, Broido DA. Three-phonon phase space and lattice thermal conductivity in semiconductors. Journal of Physics: Condensed Matter. 2008;**20**: 165209

[17] Li W, Lindsay L, Broido DA, Stewart DA, Mingo N. Thermal conductivity of bulk and nanowire $Mg_2Si_xSn_{1-x}$ alloys from first principles. Physical Review B. 2012;**86**:174307

[18] Ziman JM. The effect of free electrons on lattice conduction. Philosophical Magazine. 1957;**2**:292

[19] Dresselhaus MS, Chen G, Tang MY, YangR LH, Wang D, et al. New directions for low-dimensional thermoelectric materials[J]. Advanced Materials. 2007;**19**:1043-1053

[20] Mao J, Liu Z, Ren Z. Size effect in thermoelectric materials. npj Quantum Materials. 2016;**1**:16028

[21] Mahan GD, Sofo JO. The best thermoelectric. Proceedings of the National Academy of Sciences of the United States of America. 1996;**93**(15): 7436

[22] Friedel J. On some electrical and magnetic properties of metallic solid solutions. Canadian Journal of Physics. 1956;**34**(12A):1190-1211

[23] Anderson PW. Localized magnetic states in metals. Physics Review. 1961; **124**(1):41

[24] Blatt FJ, Schroeder PA, Foiles CL, Greig D. Thermoelectric Power of Metals. New York: Plenum Press; 1976

[25] Heremans JP, Wiendlocha B, Chamoire AM. Resonant levels in bulk thermoelectric semiconductors. Energy & Environmental Science. 2012;**5**:5510-5530

[26] Ravich YI. Selective carrier scattering in thermoelectric materials. In: Rowe DM, editor. CRC Handbook of Thermoelectrics. Boca Raton: CRC Press; 1995. p. 67

[27] Nishio Y, Hirano T. Improvement of the efficiency of thermoelectric energy conversion by utilizing potential barriers. Japanese Journal of Applied Physics. 1997;**36**(1a):170e4.1

[28] Minnich AJ, Dresselhaus MS, Ren ZF, Chen G. Bulk nanostructured thermoelectric materials: Current research and future prospects. Energy & Environmental Science. 2009;**2**:466-479. DOI: 10.1039/b822664b

[29] Ravich II. Semiconducting Lead Chalcogenides. New York: Springer; 2013

[30] Pei YZ, LaLonde AD, Wang H, Snyder GJ. Low effective mass leading to high thermoelectric performance. Energy & Environmental Science. 2012; **5**:7963

[31] Wang H, Pei Y, LaLonde AD, Snyder GJ. Material design considerations based on thermoelectric quality factor. In: Koumoto K, Mori T, editors. Thermoelectric Nanomaterials. Berlin: Springer; 2013. p. 3

[32] Wang H, Pei Y, LaLonde AD, Snyder GJ. Weak electron–phonon coupling contributing to high thermoelectric performance in n-type PbSe. Proceedings of the National Academy of Sciences of the United States of America. 2012;**109**:9705-9709. DOI: 10.1073/pnas.1111419109

[33] Liu X, Zhu T, Wang H, Hu L, Xie H, Jiang G, et al. Low electron scattering potentials in high performance $Mg_2Si_{0.45}Sn_{0.55}$ based thermoelectric solid solutions with band convergence. Advanced Energy Materials. 2013;**3**:1238

[34] Liu ZH, Wang YM, Mao J, Geng HY, Shuai J, Wang YX, et al. Lithium doping to enhance thermoelectric performance of MgAgSb with weak electron–phonon coupling. Advanced Energy Materials. 2016;**6**:1502269

[35] Zhou J, Zhu H, Liu T-H, Song Q, He R, Mao J, et al. Large thermoelectric power factor from crystal symmetry-protected non-bonding orbital in half-Heuslers. Nature Communications. 2018;**9**:1721

[36] Esfarjani K, Chen G, Stokes HT. Heat transport in silicon from first principle calculations. Physical Review B. 2011;**84**:085204

[37] Esfarjani K, Garg J, Chen G. Modeling heat conduction from first principles. Annual Review of Heat Transfer. 2014;**17**:9-47

[38] Kittel C. Introduction to Solid State Physics. 6th ed. New York: Wiley and Sons; 1986

[39] Slack GA, Tsoukala VG. Some properties of semiconducting $IrSb_3$. Journal of Applied Physics. 1994;**76**:1665

[40] Challis LJ, Cheeke JDN, Harness JB. The thermal conductivity of indium antimonide between 1.2 and 4.0°K. Philosophical Magazine. 1962;**7**:1941-1949. DOI: 10.1080/14786436 208213857

[41] Liu Z, Mao J, Liu T-H, Chen G, Ren ZF. Nano-microstructural control of phonon engineering for thermoelectric energy harvesting. MRS Bulletin. 2018; **43**:181

[42] Biswas K, He J, Blum ID, Wu C-I, Hogan TP, Seidman DN, et al. Correction: Corrigendum: High-performance bulk thermoelectrics with all-scale hierarchical architectures. Nature. 2012;**489**:414-418. DOI: 10.1038/nature11439

[43] He, Kanatzidis MG, Dravid VP. High performance bulk thermoelectrics via a panoscopic approach[J]. Materials Today. 2013;**16**:166-176. DOI: 10.1016/j. mattod. 2013.05.004

[44] Zhao LD, Dravid VP, Kanatzidis MG. The panoscopic approach to high performance thermoelectrics[J]. Energy & Environmental Science. 2014;**7**:251-268. DOI: 10.1039/c3ee43099e

[45] Klemens P. The thermal conductivity of dielectric solids at low temperatures (theoretical)[J]. Proceedings of the Physical Society, London, Section A. 1951;**208**(1092):108-133. DOI: 10.2307/98761

[46] Toberer ES, Baranowski LL, Dames C. Advances in thermal conductivity[J]. Annual Review of Materials Research. 2012;**42**:179-209

[47] Klemens P. The scattering of low-frequency lattice waves by static imperfections. Proceedings of the Physical Society, Section A. 1955;**A68**: 1113

[48] Abeles B. Lattice thermal conductivity of disordered semiconductor alloys at high temperatures[J]. Physics Review. 1963; **131**:1906

[49] Callaway J. Model for lattice thermal conductivity at low temperature[J]. Physics Review. 1959;**113**:1046

[50] Callaway J, von Baeyer HC. Effect of point imperfections on lattice thermal conductivity[J]. Physics Review. 1960; **120**:1149

[51] Klemens PG. Thermal resistance due to point defects at high temperatures[J]. Physics Review. 1960;**119**:507

[52] Abeles B, Beers D, Cody G, Dismukes J. Thermal conductivity of Ge-Si alloys at high temperatures. Physics Review. 1962;**125**:44

[53] Peierls R. On the kinetic theory of thermal conduction in crystals[J]. Annals of Physics. 1929;**3**:1055

[54] Casimir HBG. Note on the conduction of heat in crystals. Physica. 1938;**5**:495

[55] Nabarro F. The interaction of screw dislocations and sound waves. Proceedings of the Royal Society of London A. 1951;**209**:278

[56] Mingo N, Hauser D, Kobayashi NP, Plissonnier M, Shakouri A. "Nanoparticle-in-alloy" approach to efficient thermoelectrics: Silicides in SiGe. Nano Letters. 2009;**9**:711

[57] Conyers herring. Theory of the thermoelectric power of semiconductors. Physics Review. 1954;**96**:1163

[58] Zhao LD, Dravid VP, Kanatzidis MG. The panoscopic approach to high performance thermoelectrics. Energy & Environmental Science. 2014;**7**:251

[59] He Y, Lu P, Shi X, Xu F, Zhang T, Snyder GJ, et al. Ultrahigh thermoelectric performance in mosaic crystals. Advanced Materials. 2015;**27**: 3639

[60] Giustino F. Electron-phonon interactions from first principles. Reviews of Modern Physics. 2017;**89**: 015003

[61] Baroni S, de Gironcoli S, Dal Corso A, Giannozzi P. Phonons and related crystal properties from density-functional perturbation theory. Reviews of Modern Physics. 2001;**73**:515

[62] Ponce S, Margine ER, Giustino F. Towards predictive many-body calculations of phonon-limited carrier mobilities in semiconductors. Physical Review B. 2018;**97**:121201

[63] Del Sole R, Girlanda R. Optical properties semiconductors within independent-quasiparticle approximation [J]. Physical Review B. 1993;**48**:11789

[64] Gonze X, Lee C. Dynamical matrices, born effective charges, dielectric permittivity tensors, and interatomic force constants from density-functional perturbation theory. Physical Review B. 1997;**55**:10355

[65] Ma J, Nissimagoudar AS, Li W. First-principles study of electron and hole mobilities of Si and GaAs. Physical Review B. 2018;**97**:045201